Sensors & Diagnostics

PAPER

View Article Online
View Journal | View Issue

Cite this: *Sens. Diagn.*, 2024, **3**, 135

Study on inhibitory effects of AsA, $ZnCl_2$, and BAPTA-AM on Cd^{2+}-induced cell oxidative stress and cytotoxicity by scanning electrochemical microscopy (SECM) technology

Ke Gao,[a] Yuying Du,[a] Na Pan,[a] Xuewei Zhou,[a] Liping Lu *[ab] and Xiayan Wang [b]

Cadmium (Cd) can cause cell oxidative stress and cytotoxicity. Few studies have focused on inhibitory effects on Cd^{2+}-induced oxidative stress and related cytotoxicity. Scanning electrochemical microscopy (SECM) is a highly sensitive and non-invasive electrochemical analytical method. However, no information exists on inhibitory effects on Cd^{2+}-induced cell oxidative stress using SECM technology. Herein, we studied the effects of ascorbic acid (AsA), zinc chloride ($ZnCl_2$), and calcium chelator 1,2-bis (2-aminophenoxy) ethane-*N*,*N*,*N*′,*N*′-tetraacetic acid tetraethoxy methyl ester (BAPTA-AM) on cell oxidative stress with SECM. Subsequently, we studied the inhibitory effects of AsA, $ZnCl_2$, and BAPTA-AM on Cd^{2+}-induced cell oxidative stress. Consequently, 50 μmol L^{-1} AsA, 5 μmol L^{-1} $ZnCl_2$, and 5 μmol L^{-1} BAPTA-AM did not produce reactive oxygen species (ROS) and had little effect on cell viability. However, they could significantly reduce Cd^{2+}-induced excessive ROS and alleviate apoptosis ($P < 0.01$). Additionally, AsA had the strongest inhibitory effects on Cd^{2+}-induced oxidative stress, followed by BAPTA-AM and $ZnCl_2$. The inhibitory effects of AsA, $ZnCl_2$, and BAPTA-AM on Cd^{2+}-induced cytotoxicity might result from directly scavenging ROS and inhibiting oxidative stress-mediated signal transduction, enhancing antioxidant activities and maintaining cell membrane stabilities, and chelating excess calcium^{2+} (Ca^{2+}) to hinder its subsequent signal transduction, respectively. Scavenging excessive ROS and inhibiting cellular oxidative stress-mediated signal transduction might be the most effective way to alleviate Cd^{2+}-induced cytotoxicity. Our study provides empirical evidence on the inhibitory effects of AsA, $ZnCl_2$, and BAPTA-AM as specialized inhibitors against Cd^{2+}-induced cellular oxidative stress and cytotoxicity, providing precious ideas for detoxifying toxic environmental metal pollutants.

Received 16th August 2023,
Accepted 16th November 2023

DOI: 10.1039/d3sd00216k

rsc.li/sensors

1. Introduction

Heavy metal cadmium (Cd) is a non-essential element for the human body. In 2019, Cd and Cd-related substances were listed in the list of toxic and harmful water pollutants (the first batch) in China. Currently, 80–90% of Cd pollution in the environment comes from human activities,[1] including mining and industrial production. This industrial production includes synthesizing and manufacturing nickel–Cd batteries, pigments, chemical stabilizers, metal coatings, and alloys.[2] Moreover, improper discharge of Cd will likely cause environmental and public health problems due to its strong chemical activity, migration, and long-term environmental toxicity.[3] Furthermore, Cd has a long half-life, about 10–30 years in the human body.[4] Once entering the human body, Cd mainly accumulates in the liver and kidneys and causes varying degrees of damage to the lungs, bones, reproductive organs, immune system, and cardiovascular system.[5,6]

At the cellular level, Cd^{2+} can induce excessive reactive oxygen species (ROS) production, leading to oxidative stress and gradually leading to intracellular macromolecule damage, mitochondrial function inhibition, and DNA synthesis and repair dysfunction.[7–9] The accumulation of oxidative damage eventually leads to apoptosis and enhances various diseases, including diabetes, cardiovascular diseases, and arthritis.[7] Therefore, studying the inhibitory mechanisms for Cd^{2+}-induced oxidative stress and cytotoxicity is meaningful.

Several cytotoxicity mechanisms may be associated with Cd^{2+}-induced oxidative stress and cytotoxicity. Cd^{2+} can increase ROS and calcium (Ca) homeostasis imbalance in

[a] *Key Laboratory of Beijing on Regional Air Pollution Control, Department of Environmental Science, Beijing University of Technology, Beijing 100124, P.R. China. E-mail: lipinglu@bjut.edu.cn*
[b] *Center of Excellence for Environmental Safety and Biological Effects, Department of Chemistry and Biology, Beijing University of Technology, Beijing 100124, P.R. China*

cells.[10] The excessive ROS and overloaded Ca^{2+} act as second messengers to destroy proteins, lipids, and DNA in cells,[7,8] affect normal physiological activities of cells, cause organelle dysfunction, and eventually lead to autophagy, apoptosis, and tumorigenesis.[7,9] This study explores processes for inhibitory effects on Cd^{2+}-induced oxidative stress caused by the above-mentioned mechanisms.

Ascorbic acid (AsA) is necessary for all living bodies to survive and perform various physiological activities.[11] The literature has documented that AsA can be synthesized from glucose in the liver of some mammals. However, the human body lacks functional enzymes for its final synthesis.[12] Therefore, to ensure the normal physiological level of AsA in the body, humans need exogenous intake and supplementation of the required AsA from fruits and vegetables. AsA is the reduced form of vitamin C and can be used as a common antioxidant, which can react to ROS and reduce cytotoxicity.[13]

Zinc (Zn) is a trace element that plays an important role in maintaining the structural and functional stability of biological macromolecules, including proteins and enzymes.[14] Several studies have shown that Zn could inhibit Cd toxicity by competing for metal transport and binding sites of absorption proteins and maintaining the intracellular sulfhydryl content.[15,16] Specific Zn^{2+} transporters on the cell membrane can mediate the transmembrane transport of Zn^{2+}.[17] Cd^{2+} can enter cells through Zn^{2+} transporters and induce cytotoxicity due to its similar structure and charge properties.[18] Furthermore, Zn^{2+} can maintain the content of intracellular metallothionein to bind Cd^{2+} and scavenge ROS.[19]

Furthermore, 1,2-bis (2-aminophenoxy) ethane-*N*,*N*,*N*′,*N*′-tetraacetic acid tetraethoxy methyl ester (BAPTA-AM) is a highly effective Ca^{2+} ion chelator, which can inhibit the surge of intracellular Ca^{2+} concentration caused by Cd^{2+} and prevent further signal transduction by chelating with intracellular free Ca^{2+}.[20] Previous studies have shown that BAPTA-AM can alleviate the imbalance of Ca^{2+} homeostasis induced by Cd^{2+} in astrocytes and nerve cells, block mitogen-activated protein kinase (MAPK), c-Jun NH_2 terminal protein kinase (JNK) and other signaling pathways, and reduce apoptosis.[21,22]

Scanning electrochemical microscopy (SECM) is a highly sensitive electrochemical analytical method. Based on the microprobe and high-resolution positioning system, SECM technology can achieve high spatial resolution and precise positioning and image the morphology and electrochemical activity in a certain space *in situ*.[23–26] Considering its non-invasive characteristics, SECM technology has been widely used in single-cell scale research, such as cell membrane permeability research,[27–29] ROS and neurotransmitter release,[30–33] redox activity of stem cells,[34–36] multidrug resistance research,[37,38] and electroporation of yeast cells.[39]

Herein, we used SECM technology to study the inhibitory effects of AsA, zinc chloride ($ZnCl_2$), and BAPTA-AM on the ROS release of MCF-7 cells. We compared the inhibitory effects of these three substances on Cd^{2+}-induced oxidative stress. During the experiment, the H_2O_2 released by MCF-7 cells was detected using the SECM constant height scanning mode with the H_2O_2 reduction potential (−0.65 V) as the scanning voltage. Moreover, an MTT assay was used to detect the cytotoxicity of cell proliferation. Additionally, the inhibitory effects of AsA, $ZnCl_2$, and BAPTA-AM on Cd^{2+}-induced apoptosis were investigated, further confirming the reliability of SECM results.

2. Materials and methods

2.1. Chemicals

$Ru(NH_3)_6Cl_3$ (98%) was purchased from Sigma-Aldrich (Canada) and used without further purification. $CdCl_2$ was purchased from Macklin (Shanghai, China). Different concentrations of $CdCl_2$ solutions were prepared with Milli-Q water (Darmstadt, Germany) and stored at room temperature. AsA and $ZnCl_2$ were purchased from Macklin Biochemical Technology Co., Ltd. (Shanghai, China). BAPTA-AM was purchased from Sigma-Aladdin (Shanghai, China). A scanning electrochemical microscope (EIProScan), platinum ultramicroelectrode (10 μm), and Ag/AgCl reference electrode were purchased from HEKA (Germany).

2.2. Cell culture

The MCF-7 cells were obtained from the American Type Culture Collection (ATCC, Manassas, VA, USA). The cell culture medium (DMEM/high glucose), fetal bovine serum (FBS), trypsin, antibiotics, and phosphate-buffered saline (PBS) were purchased from GEN-VIEW (USA). The cell culture dishes were obtained from SOFRA (Zhejiang, China). All MCF-7 cells were incubated in a 37 °C incubator (Sanyo, Japan) containing 5% CO_2 for at least 12 h before the SECM experiments.

It has been reported that the dietary Cd intake in China was 5.3 mg kg_{BW}^{-1} per week. The annual increase in Cd concentration in adult blood was calculated to be 32.9 μmol L^{-1}. The $CdCl_2$-treated MCF-7 cells were incubated in $CdCl_2$ for 2 h before the SECM experiments to make the experimental results universal. All cells were washed with 1× PBS thrice and refilled with 2 mL 1× PBS before the SECM experiments.

The cells in the experimental group for the study on combined effects were treated as follows: MCF-7 cells were cultured in a medium containing AsA (50, 100, 150, 200 μmol L^{-1}), $ZnCl_2$ (5, 10, 20, 50 μmol L^{-1}), and BAPTA-AM (5, 10, 20, 40 μmol L^{-1}) for 2 h, to determine the concentration of AsA, $ZnCl_2$ and BAPTA-AM for the study on combined effects. MCF-7 cells were cultured in a medium containing AsA and $CdCl_2$, $ZnCl_2$ and $CdCl_2$, and BAPTA-AM and $CdCl_2$ for 2 h, respectively.

2.3. SECM experiment

Previously, the SECM feedback mode was applied to detect cell ROS. At a constant scanning height, the substrate morphology (cell height) hindered the diffusion of dissolved oxygen, resulting in a decrease in the current above the cell. The increased current value above MCF-7 cells was calculated according to the current curve in the horizontal direction (Δi). Δi is the maximum X-scan current subtracted by the baseline current, which is extracted from the 2D *in situ* scanning imaging data. And considering that the current of the system is in picoamperes, the residual current of nitrogen-deoxidized PBS is also subtracted from the current value in the 2D scan data. Moreover, the concentration–Δi increment curve was used to explore the oxidative toxicity of AsA, $ZnCl_2$, and BAPTA-AM to the cells.

The experimental methodology employed in the SECM study was derived from our previous investigation.[37] The culture dish was fixed with MCF-7 cells on the SECM scanning table. A 10 μm platinum ultramicroelectrode, Ag/AgCl reference electrode, and platinum wire counter electrode were then positioned. The three-dimensional displacement control system was used to adjust the position of the probe to make the probe tip immersed in the liquid surface. The H_2O_2 reduction potential (−0.65 V) was the working potential to make an automatic approximating curve. After stopping the approach, the tip–substrate distance was lifted by 30 μm. Then, the probe was manually approached, descended to the bottom of the plate, and brought into contact with the bottom.

Consequently, the probe was lifted by 12 μm, and the scanning operation was performed at a constant height. The tip–substrate distance and cell position were observed using a microscope, and the tip–substrate distance was moved to the vicinity of the cell for horizontal scanning (X-scan) and *in situ* imaging. The scanning speed was set at 10 μm s^{-1}, and the number of sampling points for horizontal scanning was set at 5 μm.

2.4. Cell viability

The effects of $CdCl_2$ on MCF-7 cell viability were assessed by an MTT assay. A total of 2×10^4 cells per well were seeded in a 96-well plate for 24 h and cultured in a constant-temperature incubator at 37 °C with 5% CO_2. Then, the MCF-7 cells were exposed to $CdCl_2$ for 2 h. The absorbance was detected using a microplate reader (Tecan Spark 10 M, Switzerland) at 570 nm.

2.5. Statistical analysis

All data were reported as mean ± standard deviation. The two-dimensional and three-dimensional images could directly reflect the release of ROS. The two-dimensional image of cells was drawn using Origin 2019b software, and the chroma bar represented the current level, and the three-dimensional image was drawn using Gwyddion software. The statistical significance of the differences was analyzed using GraphPad Prism 9.3. When statistically significant differences ($p < 0.05$) were found from one-way analysis of variance (ANOVA), Tukey's honestly significant difference *post hoc* test was used to determine which treatments were significantly different from one another.

3. Results and discussion

3.1. Effect of $CdCl_2$ on MCF-7 cells

Previously, we studied the effect of $CdCl_2$ on MCF-7 breast cancer cell oxidative stress.[40] At a working potential of −0.65 V, SECM was used to detect ROS release from MCF-7 cells incubated with different concentrations of $CdCl_2$ for 2 h. Under the stimulation of $CdCl_2$, the release of ROS from MCF-7 cells was concentration- and time-dependent. Following continued elevation in Cd^{2+} exposure concentration and time, the cells would undergo significant oxidative damage, impairing the antioxidant defense system. Consequently, the ATP content and pH decreased, resulting in insufficient energy supply for cellular processes. This led to dysfunction of mitochondria and other organelles, as well as a decrease in ROS production, eventually leading to

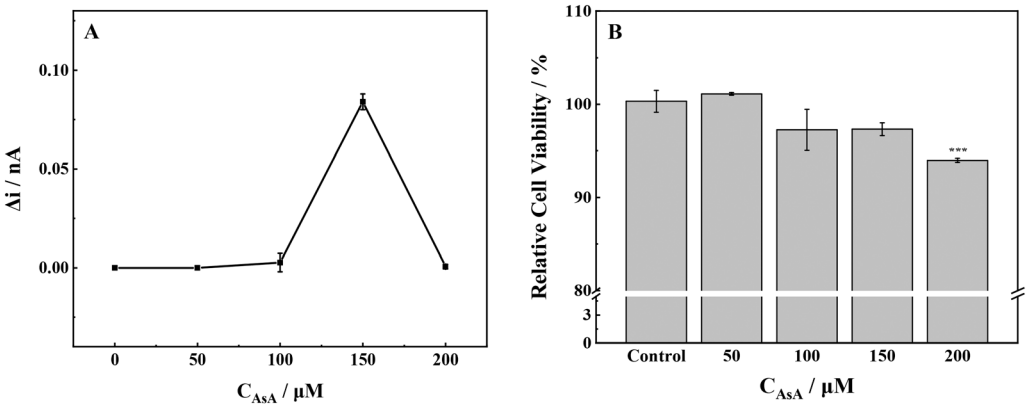

Fig. 1 (A) ROS production and (B) cell viability of MCF-7 cells with stimulation of different concentrations of AsA. ***$p < 0.001$.

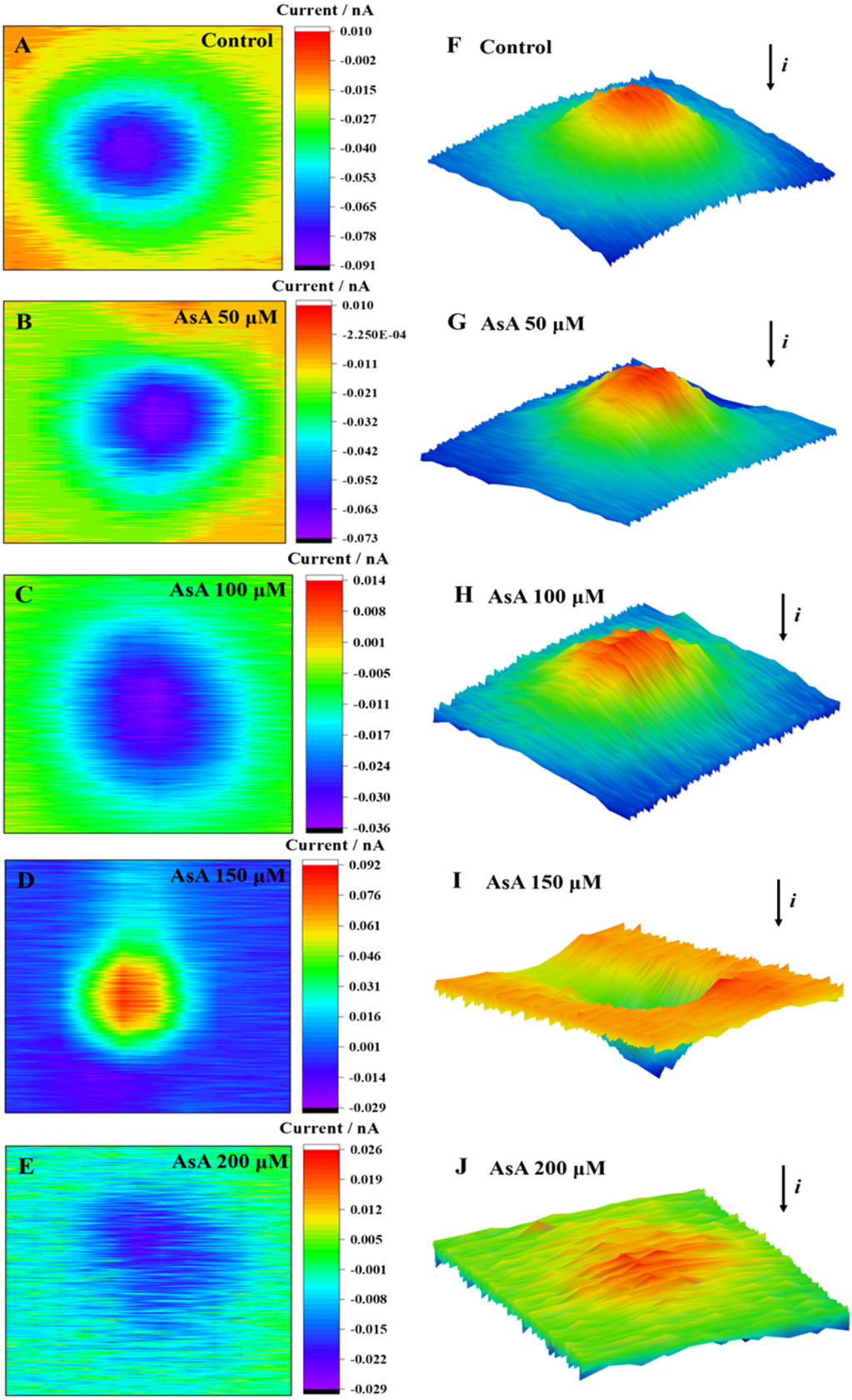

Fig. 2 2D images (A–E) and 3D images (F–J) of MCF-7 cells after incubation with AsA at different concentrations for 2 h.

apoptosis. Therefore, the Cd^{2+} concentration was fixed at 60 μmol L^{-1}. To determine the optimal concentration, we first studied the effects of different concentrations of AsA, $ZnCl_2$, and BAPTA-AM on the cell oxidative stress of MCF-7 cells. To observe the inhibitory effects of AsA, ZnCl2, and BAPTA-AM on Cd toxicity, we should also ensure that AsA, ZnCl2, and BAPTA-AM did not cause the release of ROS in cells.

3.2. Effect of AsA on MCF-7 cells

No ROS was detected outside the cells under the experimental conditions where the AsA concentration was 50 μmol L^{-1}. Conversely, when the AsA concentration was increased to 100 μmol L^{-1}, a small amount of ROS was produced in the cell and subsequently discharged into the extracellular milieu (Fig. 1A). However when the exposure concentration rose to 150 μmol L^{-1}, AsA stimulated the cells to undergo oxidative stress, the intracellular redox balance was broken, and the release of ROS increased significantly. The release of ROS returned to a lower level as the AsA concentration reached 200 μmol L^{-1}.

The proliferation toxicity of MCF-7 cells exposed to AsA was detected (Fig. 1B). At an AsA incubation concentration of 50 μmol L^{-1}, the cell viability increased slightly. However, the cell viability decreased significantly when the exposure concentration continued to increase. The changes in cell viability confirmed the results of the SECM experiment; low levels of ROS in cells were conducive to cell survival and proliferation. Conversely, high levels of ROS could cause oxidative damage to biological macromolecules, including cell protein and DNA, and further induce apoptosis. The above-mentioned experimental phenomenon was consistent with the previous literature: at low concentrations and normal physiological pH, AsA has antioxidant activity. AsA can maintain the normal physiological function of cells.[13,22] However, the high concentration of AsA can promote oxidation and induce cells to produce H_2O_2, which can destroy the redox balance of cells by changing the level of intracellular glutathione and ultimately lead to apoptosis.[22]

The cell area in two-dimensional (2D) and three-dimensional (3D) images only showed a decrease in current when the AsA incubation concentration was set at 0 μmol L^{-1}, 50 μmol L^{-1}, 100 μmol L^{-1}, and 200 μmol L^{-1} (Fig. 2). Meanwhile, current imaging could reflect the cell morphology to a certain extent. The 2D and 3D imaging of cells in the control group (0 μmol L^{-1}) presented smooth cell surface clear imaging, and no ROS were detected (Fig. 2A and F). No excessive production of ROS was detected above the cells at AsA incubation concentrations of 50 and 100 μmol L^{-1}. The cell imaging was clear, and the surface was uniform, which indicated that the cells were in good condition at these concentrations. A significant increase in current was observed above the cell area when the concentration of AsA incubation reached 150 μmol L^{-1} (Fig. 2D and I).

Meanwhile, the cell was subjected to oxidative stress, and excessive ROS were released outside the cell, resulting in a rising positive feedback current. Upon reaching a concentration increase of 200 μmol L^{-1}, the cellular 2D images were disorderly (Fig. 2E and J). The surface clarity of cells was significantly reduced, and the current in the 3D images was not significantly decreased. Therefore, it was speculated that the cell structure was damaged, the cell membrane was seriously damaged, and the blocking effect of the cell on the current was decreased.

Briefly, MCF-7 cells in low concentrations (50 μmol L^{-1}) of AsA did not produce ROS, and AsA could promote cell growth. An elevated concentration of AsA (≥150 μmol L^{-1}) could induce cell oxidative stress, produce excessive ROS, induce changes in the cell morphology, and lead to rupture of the cell membrane. This process could be attributed to the excessive release of protein kinase C signal transduction[41] and cytosolic Ca^{2+} induced by high concentrations of AsA.[42] Subsequently, the intracellular redox balance and Ca^{2+} homeostasis were broken, resulting in the overproduction of ROS and Ca^{2+}, and the cells were subjected to oxidative stress. The accumulation of oxidative damage further led to the dysfunction of organelles and ultimately led to apoptosis.

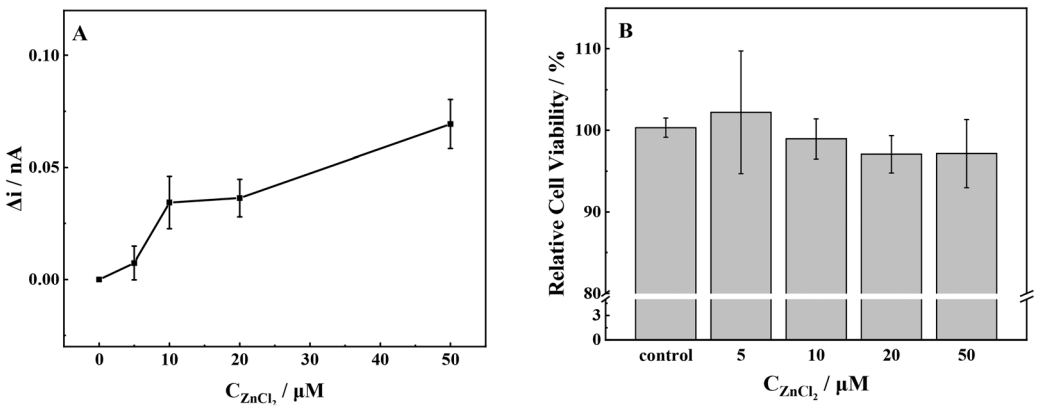

Fig. 3 (A) ROS production and (B) cell viability of MCF-7 cells with stimulation of different concentrations of $ZnCl_2$.

3.3. Effect of $ZnCl_2$ on MCF-7 cells

The gradual increase in the release of ROS from cells was observed with the increase in $ZnCl_2$ concentration from 10 μmol L^{-1} to 50 μmol L^{-1} (Fig. 3a). The release of ROS exhibited a slight increase when the concentration of $ZnCl_2$ was 5 μmol L^{-1}. Conversely, when the exposure concentration reached 10 μmol L^{-1}, lower levels of ROS could promote cell survival and delay aging.[43] The release of ROS in MCF-7 cells was significantly increased, the intracellular redox balance was broken, and the cells underwent oxidative stress. As the concentration of $ZnCl_2$ was further increased, an accompanying increase in ROS was detected. Once the concentration exceeded the cell tolerance threshold, the cell

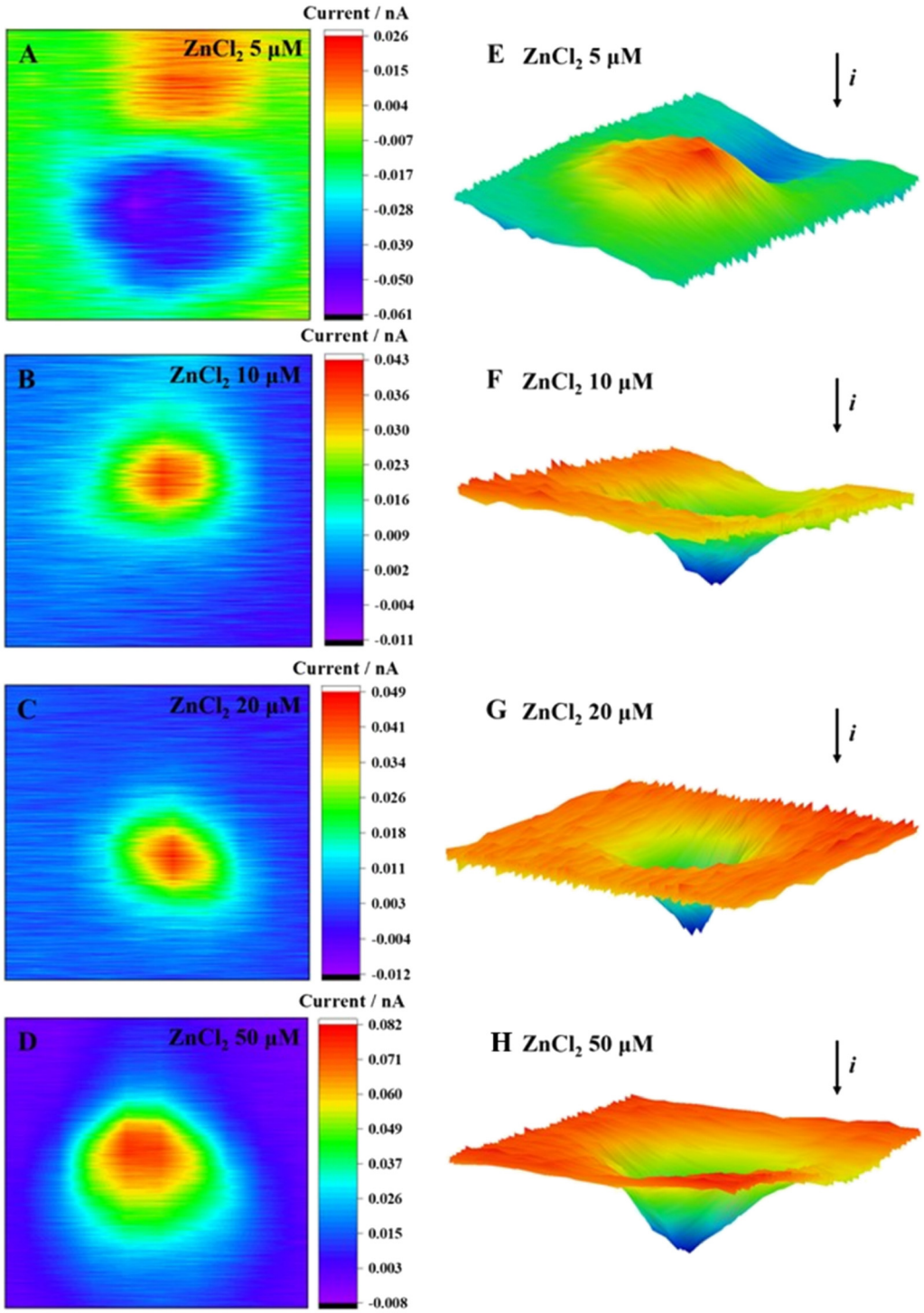

Fig. 4 2D images (A–D) and 3D images (E–H) of MCF-7 cells after incubation with $ZnCl_2$ at different concentrations for 2 h.

viability decreased.[44] Simultaneously, mitochondria were damaged by oxidation, and the ATP synthesized by mitochondria could not maintain the normal operation of cells.[45]

According to the 2D and 3D imaging of cells, the ROS release of MCF-7 cells was visualized. When the $ZnCl_2$ exposure concentration was 5 μmol L^{-1}, the cell imaging showed the blocking effect of the basal topography on the current, thereby observing the cell morphology (Fig. 4E). By comparison of the cell morphology with an unexposed group (Fig. 2A and F), the cell imaging was clear. The surface was smooth and uniform, indicating that the cell was in good condition. When the incubation concentration increased, the release of ROS from cells increased. The positive feedback current caused by H_2O_2 reduction was detected above the cell area, and the current increment gradually increased.

The Zn^{2+} competed with Cd^{2+} for the binding sites of metal transport and absorption proteins by its similar structure to that of Cd^{2+}, which might reduce the Cd^{2+}-induced cytotoxicity. At a Zn^{2+} concentration of 5 μmol L^{-1}, the cells exhibited a reduced production of ROS, thereby creating a favorable environment for cellular growth and proliferation, as evidenced by the increased cell viability. The elevation in Zn^{2+} concentration resulted in a significant increase in extracellular ROS production and a steady decline in cellular activity. Our results were consistent with the report in the literature, namely, a high concentration of Zn^{2+} leads to the decrease of mitochondrial membrane potential, dysfunction, and inability to synthesize sufficient ATP.[46] This, in turn, leads to nuclear condensation and DNA fragmentation and ultimately triggers apoptosis and necrosis.[47]

3.4. Effect of BAPTA-AM on MCF-7 cells

Outside the cells, minimal levels of ROS were detected when the concentration of BAPTA-AM was below 10 μmol L^{-1} (Fig. 5). Upon reaching a concentration of 20 μmol L^{-1}, there was a significant increase in ROS production from MCF-7 cells. When the concentration was increased to 40 μmol L^{-1}, there was a significant reduction in extracellular ROS production, approaching zero.

At low exposure concentrations (≤10 μmol L^{-1}), the release of ROS was low, and the cell viability was slightly decreased. At an incubation concentration of 20 μmol L^{-1}, the release level of ROS was the highest. Consequently, the cells underwent oxidative stress, and the cell viability decreased significantly, about 79% compared with the control group. Upon increasing the incubation concentration to 40 μmol L^{-1}, the cells were seriously damaged by oxidation, and the cell viability decreased to about 55% compared with the control group. As a membrane-permeable Ca^{2+} chelator, BAPTA-AM could break the intracellular calcium homeostasis and inhibit Ca^{2+}-mediated potassium ion channels, resulting in abnormal ion exchange inside and outside the cell.[40] Briefly, at low incubation concentrations (≤10 μmol L^{-1}), BAPTA-AM had low cytotoxicity to cells, and the redox state in cells was stable. Therefore, the physiological function of cells was normal. However, at high BAPTA-AM exposure concentrations, the redox balance and ion homeostasis of cells were broken, which might result in oxidative stress, severe oxidative damage in cells, and eventually apoptosis.

The SECM 2D and 3D imaging can reflect cell morphological changes to a certain extent (Fig. 6). When the concentration of BAPTA-AM was 5 μmol L^{-1}, an obvious current drop above the cell area was observed, which was reflected by the blocking effect of the base morphology (cell height) on the steady-state current. Meanwhile, the cell imaging was clear, and the surface was smooth. Upon increasing the concentration of BAPTA-AM to 10 μmol L^{-1}, the cell morphology was changed, and ridge-like folds appeared on the surface. As the concentration increased to 20 μmol L^{-1}, cellular oxidative stress was observed, releasing excessive ROS into the extracellular environment. A positive feedback current caused by H_2O_2 reduction was also detected above the cell area. Once the exposure

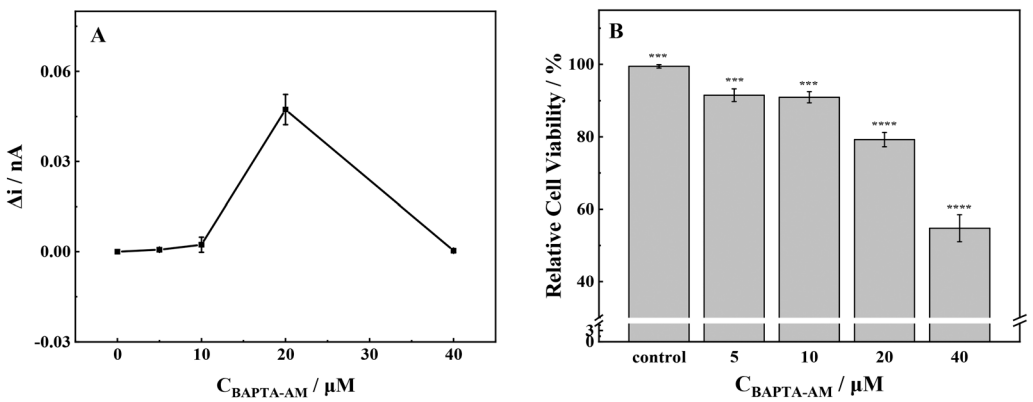

Fig. 5 (A) ROS production and (B) cell viability of MCF-7 cells with stimulation of different concentrations of BAPTA-AM. Note: ***$p < 0.001$, ****$p < 0.0001$.

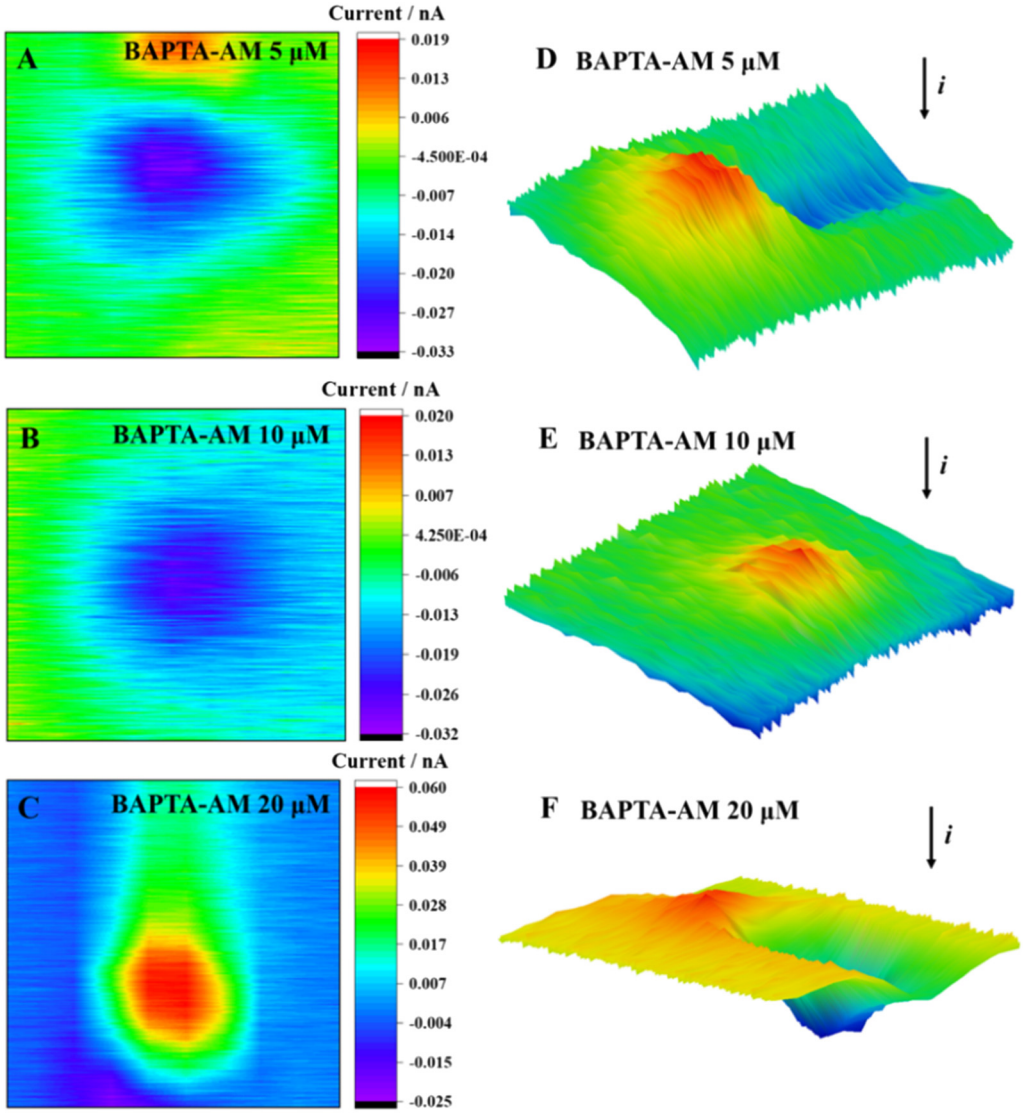

Fig. 6 2D images (A–C) and 3D images (D–F) of MCF-7 cells after incubation with BAPTA-AM at different concentrations for 2 h.

concentration of BAPTA-AM increased to 40 μmol L^{-1}, the MCF-7 cells exhibited poor viability, resulting in their detachment from the culture dish during the scanning process. Consequently, it was challenging to obtain complete imaging.

As a common Ca^{2+} chelator, BAPTA-AM can alleviate the surge of intracellular Ca^{2+} levels caused by Cd^{2+} and effectively reduce the cell dysfunction and death caused by Cd^{2+}. Under incubation with a lower concentration of BAPTA-AM (≤5 μmol L^{-1}), only a very low level of ROS was detected outside the cell, and the cell viability was not significantly decreased. With the increase in concentration, BAPTA-AM inhibited the potassium ion channel on the membrane, which might cause the disorder of the intracellular ion state, which destroyed the balance between the production and elimination of ROS in the cell.[21,22] High levels of ROS led to oxidative stress in the cell and, eventually, apoptosis.

3.5. Inhibitory effects of AsA, $ZnCl_2$, and BAPTA-AM on Cd-induced oxidative stress

Herein, we investigated the combined effects of AsA, $ZnCl_2$, and BAPTA-AM with $CdCl_2$. According to previous experimental results, 50 μmol L^{-1} AsA, 5 μmol L^{-1} $ZnCl_2$, and 5 μmol L^{-1} BAPTA-AM did not produce ROS and had little effect on cell viability. Therefore, the above concentrations of AsA, $ZnCl_2$, and BAPTA-AM were selected to study their effects on oxidative stress induced by $CdCl_2$ in MCF-7 cells. SECM was used to detect the ROS release of MCF-7 cells under the joint action of the above-mentioned three elements and $CdCl_2$ (Fig. 7). The application of the three inhibitors resulted in a significant decrease in the release of ROS in MCF-7 cells when compared with $CdCl_2$. This reduction in ROS levels suggests that AsA, ZnCl2, and BAPTA-AM could effectively inhibit the oxidative stress induced by $CdCl_2$. Among them, AsA had the strongest inhibitory effect on the oxidative stress

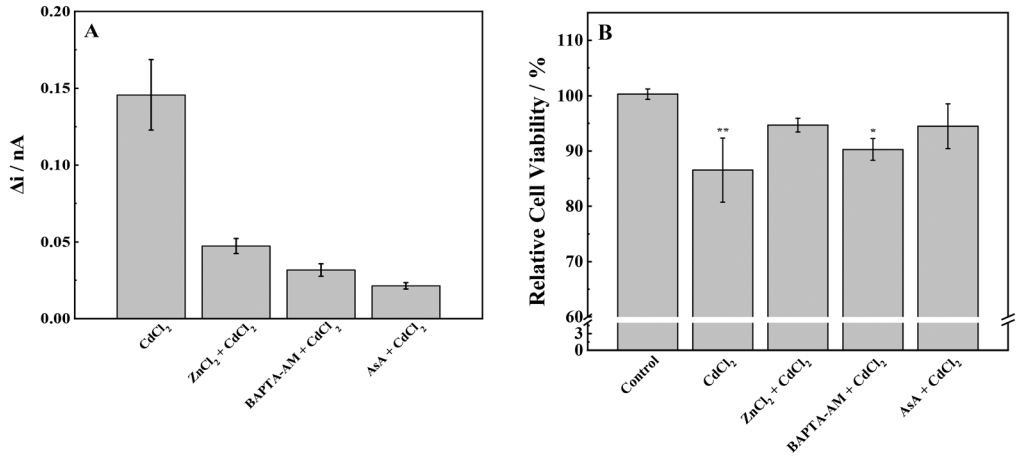

Fig. 7 (A) ROS production and (B) cell viability of MCF-7 cells with stimulation of $CdCl_2$ and inhibitors. Note: *$p < 0.05$, **$p < 0.01$.

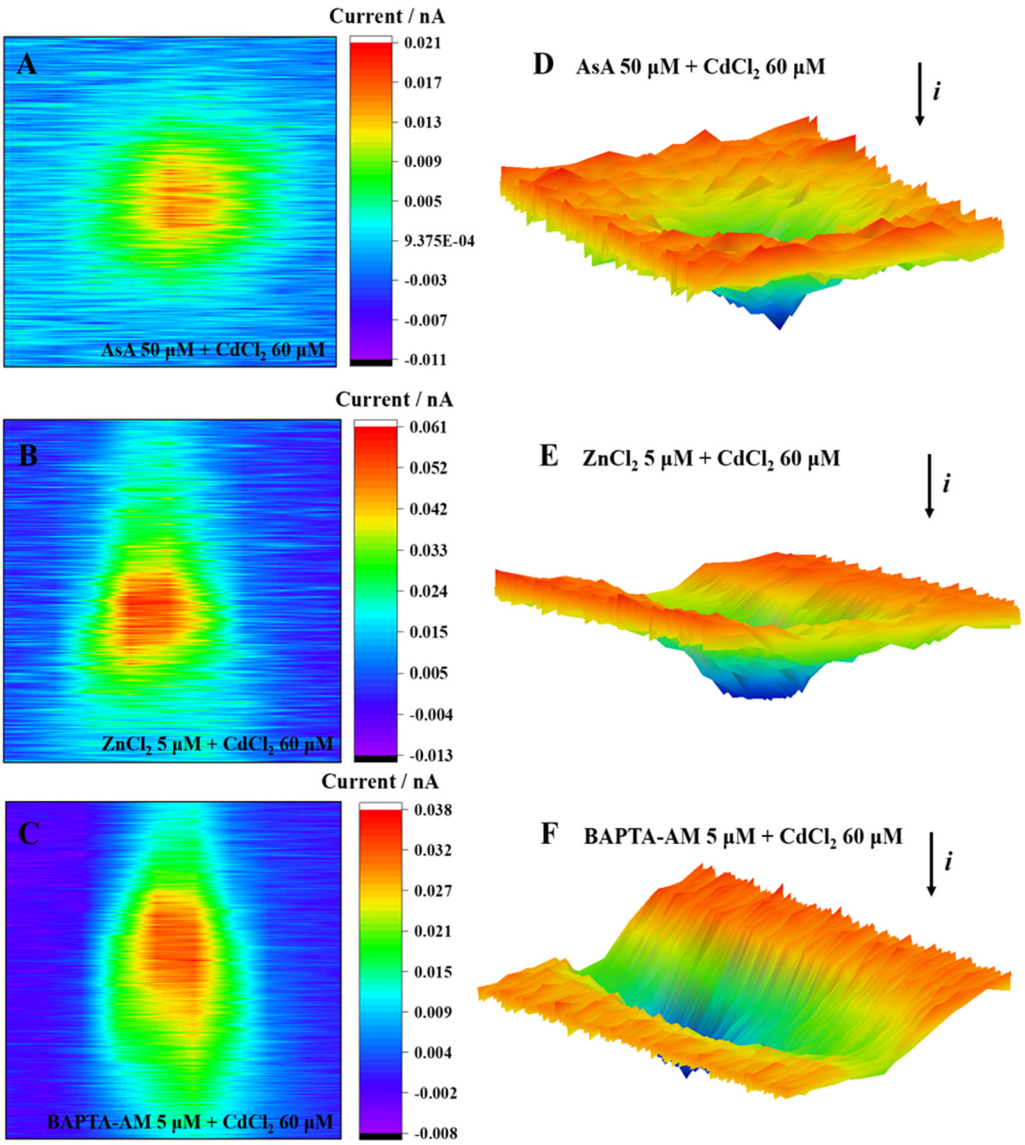

Fig. 8 2D images (A–C) and 3D images (D–F) of MCF-7 cells after incubation with $CdCl_2$ and inhibitors.

induced by $CdCl_2$, followed by BAPTA-AM, and $ZnCl_2$ had the weakest inhibitory effect. These results are consistent with published papers showing that ASA can reduce ROS caused by Cd^{2+}, while inhibiting the phosphorylation of p38 MAPK and the translocation of AIF protein (from mitochondria to the nucleus) to reduce the damage of Cd^{2+} to cells; zinc can also inhibit Cd-induced ROS production, and furthermore can inhibit Cd accumulation in cells;[48,49] BAPTA-AM as a chelating agent can remove the Cd-induced intracellular Ca^{2+} increase, and Ca^{2+} mediates calpain activation and intracellular ROS production.[50] BAPTA-AM also inhibits Cd-induced mitochondrial depolarization and caspase activation.[51,52]

To further prove the reliability of the SECM experiment, the MTT method was used to detect the cytotoxicity of cell proliferation under the combined action of an inhibitor and Cd. It is consistent with the results of SECM studies: 60 μmol L^{-1} $CdCl_2$ significantly reduced the cell activity, and adding an inhibitor alleviated the cytotoxicity of Cd to a certain extent and improved the cell viability by reducing oxidative stress.

Fig. 8 shows the ROS release of MCF-7 cells under the combined exposure to an inhibitor and $CdCl_2$. The positive feedback current caused by H_2O_2 reduction was detected above the cell area; the cells were subjected to oxidative stress, and the intracellular ROS were overproduced. Moreover, many studies have shown that appropriate levels of AsA can inhibit oxidative stress-mediated signal transduction, including animal rapamycin target protein (mTOR)[48] and mitogen-activated protein kinase (MAPK).[53] Typically, 5 μmol L^{-1} $ZnCl_2$ can alleviate the oxidative stress induced by $CdCl_2$ by promoting the activities of intracellular antioxidants SOD and GSH, reducing ROS generation and subsequently restoring cell viability.[54] Furthermore, Zn, as a biologically essential trace element, plays a key role in the catalytic and structural functions of various proteins.[55] Zn can maintain the stability of the cell membrane,[56] alleviating cadmium-induced mitochondrial depolarization.[57] Briefly, 5 μmol L^{-1} BAPTA-AM could penetrate cells, chelate excess Ca^{2+} released by cells under cadmium stimulation, and subsequently inhibit the Ca^{2+}-mediated signaling pathway. To date, several studies have shown an interaction between Ca^{2+} and ROS:[57,58] maintaining the normal Ca^{2+} level of the cell is conducive to the stability of the redox state in the cell, consequently ensuring the normal operation of mitochondria and other organelles.[59]

Low concentrations of AsA, $ZnCl_2$, and BAPTA-AM could inhibit the oxidative stress induced by Cd, restore cell viability, and alleviate the cytotoxicity of Cd (Fig. 9). Their action pathways were observed to have a direct impact on the scavenging of ROS and the inhibition of signal transduction mediated by oxidative stress. This resulted in improving antioxidant activity and maintaining cell membrane stability. Additionally, they can chelate excessive Ca^{2+} to hinder its subsequent signal transduction. Comparing the effects of removing ROS and restoring cell viability, AsA had the best inhibitory effect on Cd^{2+}-induced cytotoxicity.

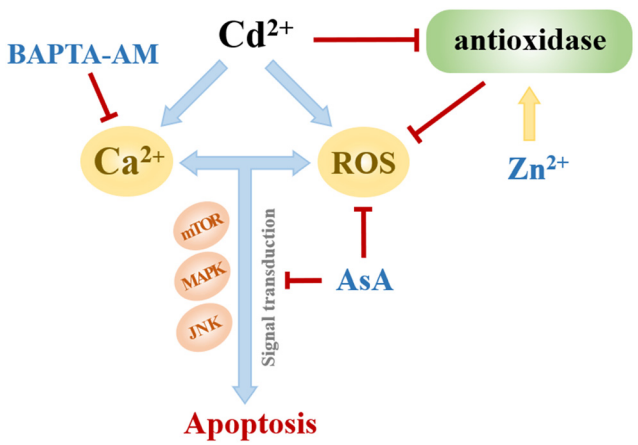

Fig. 9 Effects of AsA, $ZnCl_2$ and BAPTA-AM on Cd^{2+}-induced oxidative stress.

4. Conclusion

Herein, SECM technology was used to detect the ROS release of MCF-7 cells under exposure to AsA, $ZnCl_2$, and BAPTA-AM. Moreover, the toxic effects of these three substances on cells were studied in combination with cell proliferation toxicity experiments. According to the cell exposure experiments of different concentrations of AsA, $ZnCl_2$, and BAPTA-AM, the action concentrations of these three inhibitors in the follow-up studies were determined, including 50 μmol L^{-1} AsA, 5 μmol L^{-1} $ZnCl_2$, and 5 μmol L^{-1} BAPTA-AM. The effects of these three inhibitors on Cd^{2+}-induced oxidative stress and apoptosis were investigated. The results showed that at low concentrations, the three inhibitors could reduce the excessive ROS produced by Cd^{2+}-induced cells and alleviate the apoptosis caused by Cd^{2+} by inhibiting oxidative stress. Among these three inhibitors, AsA had the strongest inhibitory effect on Cd^{2+}-induced oxidative stress, followed by BAPTA-AM and $ZnCl_2$. Scavenging excessive ROS and inhibiting cellular oxidative stress may be the most effective way to alleviate Cd^{2+}-induced cytotoxicity.

Author contributions

All authors contributed to the study conception and design. Material preparation, data collection and analysis were performed by Ke Gao, Na Pan, Xuewei Zhou and Yuying Du. The first draft of the manuscript was written by Ke Gao and all authors commented on previous versions of the manuscript. Review and editing, supervision, and funding acquisition were performed by Liping Lu and Xiayan Wang.

Conflicts of interest

The authors have no relevant financial or non-financial interests to disclose.

Acknowledgements

This work was financially supported by the National Natural Science Foundation of China (No. 22206009, 22276005, 21876005) and the Beijing Outstanding Young Scientist Program (BJJWZYJH01201910005017).

References

1 Y. Zhao, Q. Deng, Q. Lin, C. Zeng and C. Zhong, *Environ. Pollut.*, 2020, **263**, 114338.
2 X. Zhang, T. Zhong, L. Liu and X. Ouyang, *PLoS One*, 2015, **10**, e0135182.
3 Y. Wu, X. Yang, H. Wang, G. Jia and T. Wang, *J. Hazard. Mater.*, 2021, **403**, 123871.
4 R. K. Zhang, P. Wang, Y. C. Lu, L. Lang, L. Wang and S. C. Lee, *J. Cell. Physiol.*, 2019, **234**, 18230–18248.
5 P. B. Tchounwou, C. G. Yedjou, A. K. Patlolla and D. J. Sutton, *Exper. Suppl.*, 2012, **101**, 133–164.
6 L. Järup, Hazards of heavy metal contamination, *Br. Med. Bull.*, 2003, **68**, 167–182.
7 G. Genchi, M. S. Sinicropi, G. Lauria, A. Carocci and A. Catalano, *Int. J. Environ. Res. Public Health*, 2020, **17**, 3782.
8 A. R. Nair, O. Degheselle, K. Smeets, E. Van Kerkhove and A. Cuypers, *Int. J. Mol. Sci.*, 2013, **14**, 6116–6143.
9 W. K. Lee and F. Thévenod, *Arch. Toxicol.*, 2020, **94**, 1017–1049.
10 X. Zhou, W. Hao, H. Shi, Y. Hou and Q. Xu, *Oncol. Res. Treat.*, 2015, **38**, 311–315.
11 I. Mellidou and A. K. Kanellis, *Front. Chem.*, 2017, **5**, 50.
12 M. Y. Lachapelle and G. Drouin, *Genetica*, 2011, **139**, 199–207.
13 A. Chakraborty and N. R. Jana, *ACS Appl. Mater. Interfaces*, 2017, **9**, 41807–41817.
14 D. Zhang, J. Liu, J. Gao, M. Shahzad, Z. Han, Z. Wang, J. Li and H. Sjölinder, *PLoS One*, 2014, **9**, e103427.
15 M. M. Rahman, K. F. B. Hossain, S. Banik, M. T. Sikder, M. Akter, S. E. C. Bondad, M. S. Rahaman, T. Hosokawa, T. Saito and M. Kurasaki, *Ecotoxicol. Environ. Saf.*, 2019, **168**, 146–163.
16 S. D. Francis Stuart and A. R. Villalobos, *Int. J. Mol. Sci.*, 2021, **22**, 8857.
17 A.-G. Desbrosses-Fonrouge, K. Voigt, A. Schröder, S. Arrivault, S. Thomine and U. Krämer, *FEBS Lett.*, 2005, **579**, 4165–4174.
18 S. Satarug, S. Garrett, S. Somji, M. Sens and D. J. T. Sens, *Toxics*, 2021, **9**, 94.
19 V. Kloubert and L. Rink, *Food Funct.*, 2015, **6**, 3195–3204.
20 Z. Cao, D. Liu, Q. Zhang, X. Sun and Y. Li, *Biol. Trace Elem. Res.*, 2016, **169**, 247–253.
21 J. H. Jiang, G. Ge, K. Gao, Y. Pang, R. C. Chai, X. H. Jia, J. G. Kong and A. C.-H. Yu, *Neurochem. Res.*, 2015, **40**, 1929–1944.
22 M. Uetaki, S. Tabata, F. Nakasuka, T. Soga and M. Tomita, *Sci. Rep.*, 2015, **5**, 13896–13904.
23 N. Pan, K. Gao, B. Zhang, X. Fan, L. Lu and X. Wang, *Sci. Total Environ.*, 2022, **833**, 155208.
24 A. J. Bard, X. Li and W. Zhan, *Biosens. Bioelectron.*, 2006, **22**, 461–472.
25 Y. Zhao, Y. Li, S. Kuermanbayi, Y. Liu, J. Zhang, Z. Ye, H. Guo, K. Qu, F. Xu and F. Li, *Anal. Chem.*, 2023, **95**, 1940–1948.
26 M. Nebel, S. Grützke, N. Diab, A. Schulte and W. Schuhmann, *Angew. Chem., Int. Ed.*, 2013, **52**, 6335–6338.
27 M. S. M. Li, F. P. Filice, J. D. Henderson and Z. Ding, *J. Phys. Chem. C*, 2016, **120**(11), 6094–6103.
28 F. P. Filice, M. S. M. Li, J. D. Henderson and Z. Ding, *Anal. Chim. Acta*, 2016, **908**, 85–94.
29 B. Zhang, N. Pan, X. Fan, L. Lu and X. Wang, *Analyst*, 2021, **146**, 5973–5979.
30 M. Shen, Z. Qu, J. DesLaurier, T. M. Welle, J. V. Sweedler and R. Chen, *J. Am. Chem. Soc.*, 2018, **140**, 7764–7768.
31 H. S. C. Sáenz, L. P. Hernández-Saravia, J. S. G. Selva, A. Sukeri, P. J. Espinoza-Montero and M. Bertotti, *Microchim. Acta*, 2018, **185**, 367.
32 S. E. Salamifar and R. Y. Lai, *Anal. Chem.*, 2013, **85**, 9417–9421.
33 Y. Li, K. Hu, Y. Yu, S. A. Rotenberg, C. Amatore and M. V. Mirkin, *J. Am. Chem. Soc.*, 2017, **139**, 13055–13062.
34 D. Bironaite, J. Petroniene, R. Miksiunas, A. Zinovicius, I. Morkvenaite-Vilkonciene and A. Ramanavicius, *Electrochim. Acta*, 2023, **455**, 142389.
35 J. Petroniene, I. Morkvenaite-Vilkonciene, R. Miksiunas, D. Bironaite, A. Ramanaviciene, L. Mikoliunaite, A. Kisieliute, K. Rucinskas, V. Janusauskas, I. Plikusiene, S. Labeit and A. Ramanavicius, *Electroanalysis*, 2020, **32**, 1337–1345.
36 J. Petroniene, I. Morkvenaite-Vilkonciene, R. Miksiunas, D. Bironaite, A. Ramanaviciene, K. Rucinskas, V. Janusauskas and A. Ramanavicius, *Electrochim. Acta*, 2020, **360**, 136956.
37 S. Kuss, D. Polcari, M. Geissler, D. Brassard and J. Mauzeroll, *Proc. Natl. Acad. Sci. U. S. A.*, 2013, **110**, 9249–9254.
38 D. Polcari, J. HernáNdez-Castro, K. Li, M. Geissler and J. J. A. C. Mauzeroll, *Anal. Chem.*, 2017, **89**, 8988–8994.
39 M. Poderyte, A. Valiunienė and A. Ramanavicius, *Biosens. Bioelectron.*, 2022, **205**, 114096.
40 N. Pan, L. Lu, B. Zhang and X. Wang, *Anal. Methods*, 2022, **14**, 2673–2681.
41 M. W. Baek, H. S. Cho, S. H. Kim, W. J. Kim and J. Y. Jung, *J. Cell. Physiol.*, 2017, **232**, 417–425.
42 G. G. Martinovich, E. N. Golubeva, I. V. Martinovich and S. N. Cherenkevich, *J. Biophys.*, 2012, **2012**, 921653.
43 M. Schieber and N. S. Chandel, *Curr. Biol.*, 2014, **24**, R453–R462.
44 K. Jomova, D. Vondrakova, M. Lawson and M. Valko, Metals, *Mol. Cell. Biochem.*, 2010, **345**, 91–104.
45 J. Lemire, R. Mailloux and V. D. Appanna, *J. Appl. Toxicol.*, 2008, **28**, 175–182.
46 H. Yanagisawa, M. Sato, M. Nodera and O. Wada, *J. Hypertens.*, 2004, **22**, 543–550.

47 N. Chen, P. Su, M. Wang and Y. M. Li, *Environ. Sci. Pollut. Res.*, 2018, **25**, 21713–21720.
48 J. Kim and J. Soh, *Toxicol. Lett.*, 2009, **188**, 45–51.
49 A. Szuster-Ciesielska, A. Stachura, M. Słotwinska, T. Kaminska, R. Śnieżko, R. Paduch, D. Abramczyk, J. Filar and M. Kandefer-Szerszen, *Toxicology*, 2000, **145**, 159–171.
50 P. Yang, H. Chen, J. Tsai and L. Lin, *Chem. Res. Toxicol.*, 2007, **20**, 406–415.
51 S. H. Wang, Y. L. Shih, W. C. Ko, Y. H. Wei and C. M. Shih, *Cell. Mol. Life Sci.*, 2008, **65**, 3640–3652.
52 M. Yang, S. Teng, C. Ma, Y. Yu, P. Wang and C. J. C. Yi, *Cytotechnology*, 2018, **70**, 1301–1313.
53 A. J. Lee, J. W. Lim and H. Kim, *J. Cancer Prev.*, 2021, **26**, 64–70.
54 D. Zhang, Y. Li, T. Zhang, J. Liu, W. J. E. Tian and E. Safety, *Ecotoxicol. Environ. Saf.*, 2018, **163**, 331–339.
55 S. H. Choi, K. L. Lee, J. H. Shin, Y. B. Cho, S. S. Cha and J. H. Roe, *Nat. Commun.*, 2017, **8**, 15812.
56 M. Bicer, M. Gunay, A. K. Baltaci, K. Uney, R. Mogulkoc and M. Akil, *Bratisl. Lek. Listy*, 2012, **113**, 199–205.
57 S. Feno, G. Butera, D. Vecellio Reane, R. Rizzuto and A. Raffaello, *Oxid. Med. Cell. Longevity*, 2019, 9324018.
58 V. Demidchik and S. Shabala, *Funct. Plant Biol.*, 2018, **45**, 9–27.
59 R. Hodeify, S. S. Siddiqui, R. Matar, C. G. Vazhappilly, M. Merheb, H. Al Zouabi and J. Marton, *Heliyon*, 2021, **7**, e06041.